

A Dual AC and DC Output Flyback Converter

Luocheng Wang, *Student Member, IEEE*

Advanced Power Electronics and Electric Drives Laboratory
University of Connecticut, Storrs, CT, USA
luocheng.wang@uconn.edu

Ali M. Bazzi, *Member, IEEE*

Advanced Power Electronics and Electric Drives Laboratory
University of Connecticut, Storrs, CT, USA
alibazzi@ieee.org

Abstract—This paper presents a new flyback converter topology with dual DC and AC outputs. In traditional flyback converters, usually there are multiple secondary windings that can be utilized to construct few additional output ports. This new topology takes advantage of one of additional secondary windings to generate continuous AC voltage, accompanying with the conventional DC output voltage. In this new topology, the DC output follows the traditional configuration while the AC output is achieved by adding an L-C filter to an additional secondary winding. This new dual-output flyback converter integrates a standalone DC/DC converter with DC/AC inverter which helps save space and switching devices. The main purpose of the proposed dual-output flyback converter is to cope with more general applications especially when both DC and AC power are necessary, such as in rural solar-powered standalone systems.

Keywords—flyback transformer; flyback converter topology; DC/DC; DC/AC; discontinuous conduction mode (DCM); power converter

I. INTRODUCTION

Power electronics have recently seen significant penetration as energy conversion stages in daily applications ranging from generation, e.g., renewable energy applications, to loads e.g. electric drives and lighting ballasts and drivers. Energy conversion between DC and AC forms is critical as electrical loads and generators can provide power in either form. A power electronic converter that can provide both AC and DC regulated power outputs is thus of major interest in various applications, especially in one single converter.

In this paper, a dual-output flyback converter topology is proposed to provide both DC and AC outputs from a single DC source, which achieves the integration of DC and AC on one single converter. Typical applications of the proposed topology would be in rural energy systems such as stand-alone solar photovoltaics (PV) providing energy to simple DC loads such as batteries, and high-frequency AC loads such as fluorescent lights as illustrated in Fig.1. The choice of a flyback converter stems from its high efficiency and inherent AC conversion which is usually rectified to reach a DC output. It is also one of the most common converters in switch-mode power supplies below 200W [1]. Another feature of this converter is its electrical isolation between the input and output sides through a coupled inductor which is also known as the flyback transformer [2]. It can offer single or multiple isolated output voltages and operate over a range of input voltages [3]. The coupled inductor does not conduct current on both sides simultaneously, different from normal transformers; it stores input energy by input current, stores energy into its air gap during one portion of the switching cycle—‘ON’, and releases it to the outputs during the other

portion of the cycle—‘OFF’[1-3]. Generally, if all energy is released to the output due to a short ON cycle and long OFF cycle, the flyback operates in discontinuous conduction mode (DCM) where the primary current reaches zero compared to the continuous conduction mode (CCM) where the primary current is never zero.

The proposed dual-output flyback converter topology takes advantages of these features to construct an additional high-frequency AC output, besides traditional stable DC output. Given that many flyback transformers have multiple output windings which are rarely used concurrently, one of these windings can be dedicated to the AC port. In fact, it is sometimes more economical to purchase mass-produced multi-winding flyback transformers even for a single-output design, thus adding the AC port could come at minimal cost increase. This paper is an introduction to the dual-output flyback converter topology including the circuit, hardware prototype, power efficiency results, and preliminary modeling.

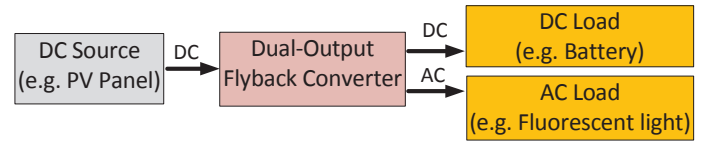


Fig.1. Application diagram of proposed dual-output flyback topology

II. PROPOSED TOPOLOGY

The proposed topology is similar to the traditional flyback converter, except that an AC output is added to an additional secondary winding of flyback transformer. The AC output conducts during all portions of a switching cycle from the primary side to give a continuous sinusoidal wave. Since the coupled-inductor inherently blocks DC current from propagating to the secondary side, only an additional second-order low-pass filter (LPF) is required on the AC side to achieve clean high-frequency AC output. The proposed topology is shown in Fig. 2.

As shown in Fig. 2, the transformer primary magnetizing inductance (L_m) is connected to a DC input voltage (V_{in}) and followed by a switching MOSFET at high frequency. This input stage is the same with traditional topology. The snubber circuit is essential to reduce the input voltage ripple and dissipate the remaining air gap energy after a switching cycle [4-6]. While the DC output port is similar to that in the traditional flyback converter, the AC output port on the right is proposed—a simple second-order LC low-pass filter is utilized to shape V_{s2} from a zero-offset square wave to a sinusoidal wave. The AC output is continuous as well since V_{s2} is continuous square waves from primary winding. The real power transferred from the AC

secondary winding to the load and the filter is ideally conserved since the latter only contains inductor and capacitor that impact reactive power. With existing control of the DC side, the AC terminal gives continuous output at the switching frequency. It is important to note that the effect of the AC side on DC output and power regulation is shown in the hardware testing results but still needs better understanding from a modeling perspective.

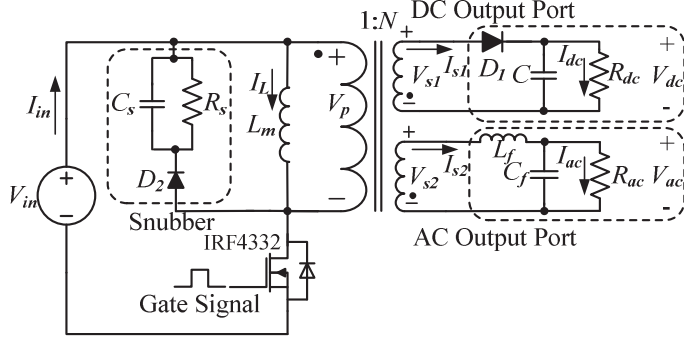


Fig.2. Proposed dual-output AC and DC flyback converter topology

The experimental prototype of Fig. 2 is shown in Fig. 3 in addition to the gate drive circuit and AC output port current sensing resistor. The converter prototype is run under open-loop control where a PWM signal is provided to the gate driver without closed-loop feedback. Loads on the DC and AC output ports are simple resistors as shown in Fig. 3. Section III elaborates on the testing results for various loads while Table I shows the values or part numbers of the components used. The duty (D) is set to 50%, the switching frequency (f) is set to 100 kHz, and the flyback turns ratio (N) is 1:0.33 per output port.

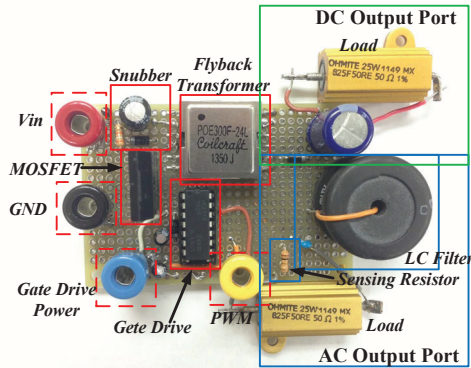


Fig.3. Hardware circuit of proposed dual-output flyback converter topology

TABLE I. Listings of partial components of hardware circuit

Name	Part Parameter
L_m	42 μ H (Coilcraft POE300F-24L)
D_1	400V, 1A (oversized)
C	220 μ F (Electrolytic)
L_f	4.7 μ H
C_f	0.22 μ F (Ceramic)
D_2	400V, 1A (oversized)
C_s	680 μ F/200V
R_s	39k Ω
R_{dc}	Power Resistor 50.4 Ω or 101 Ω
R_{ac}	Power Resistor 50.4 Ω or 101 Ω

III. EXPERIMENTAL RESULTS

A previous prototype (not shown here) suffered from low power efficiency (η) and significant AC waveform distortion even during low power operation. The prototype shown in Fig. 3 was built with minimum leads, wires, and a two-layer prototype board thus reducing board parasitic effects. This dual-output flyback converter is operated in the discontinuous conduction mode (DCM) [7, 8] which also enhances η due to less power dissipated in the snubber circuit and MOSFET.

Various resistive loads were tested at both AC and DC output ports. Results from these tests under various input voltages with open-loop control were recorded. Waveforms of one example where $V_{in}=6.5V$ and both loads being 50.4 Ω each are shown in Fig. 4 (a-d). The dual-output voltage and current values are presented in Table II.

TABLE II. Testing results of example $V_{in}=6.5V$ $R_{dc}=R_{ac}=50.4\Omega$

Input Stage		DC Output Port			AC Output Port (rms value)			η (%)
I_{in} (A)	P_{in} (W)	V_{dc} (V)	I_{dc} (mA)	P_{dc} (W)	V_{ac} (V)	I_{ac} (A)	P_{ac} (W)	
0.35	2.275	4.97	98.9	0.49	6.97	0.23	1.60	91.86

Since the AC output is a continuous sinusoidal waveform, the RMS values of its voltage and current, while the mean values of the DC output are measured. Efficiency is calculated by assuming that the total input power is conserved as losses plus the power delivered to the DC and AC loads. In the ideal situation, without any other dissipation or heat, the energy in the dual-output flyback converter is supposed to be conserved.

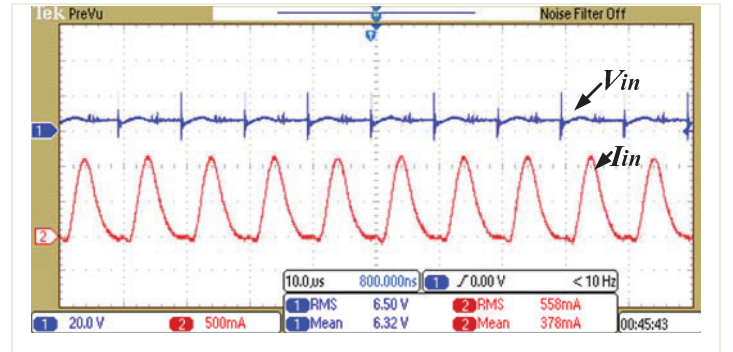


Fig.4(a). Input voltage and current waveforms with $V_{in}=6.5V$ $R_{dc}=R_{ac}=50.4\Omega$

Fig. 4(a) shows the input voltage and current waveform in this case. The DC input voltage (blue) is slightly distorted by the switching signal. The input current (red) shows that current increases during every switching cycle of 'ON' and returns to zero before every single end of switching cycle, which verifies the DCM of dual-output flyback converter operation. However, comparing dual-output to single-output flyback converter, the duty ratio (D) is affected and reduced from 50% as set on the PWM source to 35% (D_{on}) in the hardware testing. The converter takes around 25% of one period for the input current to return to zero (D_{off}), and the remaining zero-current portion of the switching period is approximately 40%. The reason why the duty ratio drops from 50% to approximately 35% is still being investigated.

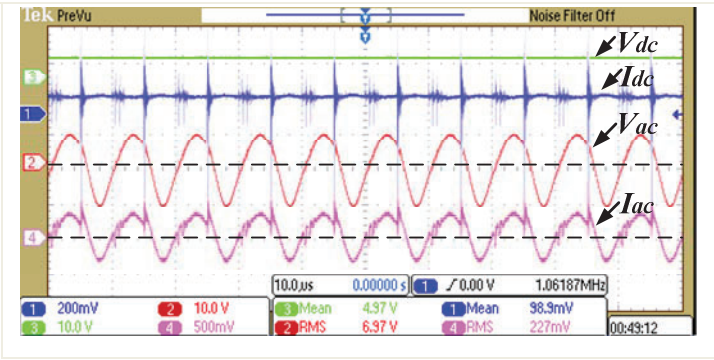


Fig.4 (b). DC and AC output waveforms with $V_{in}=6.5V$ $R_{dc}=R_{ac}=50.4\Omega$

Fig. 4(b) shows both DC and AC outputs waveforms for the example in Table II. Both DC and AC voltages are continuous and stable thus both DC and AC output ports function as expected for the proposed dual-output flyback converter. DC and AC voltages are more clear and smooth than currents as current measurements are more sensitive to switching transients.

Fig. 4(c) shows only the AC voltage and current for the example in Table II. The AC output frequency is at the switching frequency, and a sinusoidal voltage at switching frequency is achieved. The AC output current has some phase lag since the power resistor shows some inductive characteristics at 100kHz. The power resistor was characterized on a network analyzer to have $5.65\mu H$ inductance in series with 50.4Ω resistance at 100 kHz which give a 3.59° degree phase lag that can be ignored since the power factor, $\cos(3.59^\circ) \approx 0.998$.

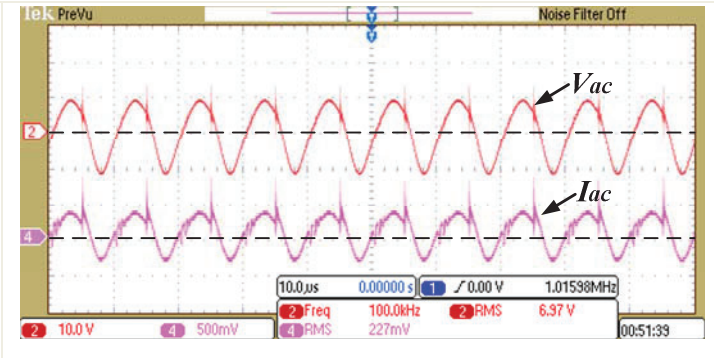


Fig.4(c). AC output voltage and current with $V_{in}=6.5V$ $R_{dc}=R_{ac}=50.4\Omega$

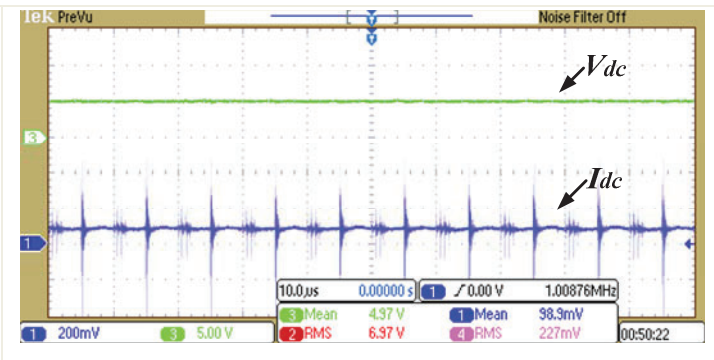


Fig.4(d). DC output voltage and current with $V_{in}=6.5V$ $R_{dc}=R_{ac}=50.4\Omega$

Fig. 4(d) shows only DC voltage and current from Table II which are similar to those in a traditional flyback converter DC output. The ratio between DC output voltage and current is

50.25Ω , relatively the same as the resistance 50.4Ω load resistor with 0.3% error.

Various input voltages and four different load combinations were tested where $R_{dc}=R_{ac}$ at 50.4Ω or 101Ω , or $R_{dc} \neq R_{ac}$ where one is 50.4Ω and the other is 101Ω . Tables III-VI present measured input and output voltages and currents along with the total converter efficiency. The average power efficiency is shown to be above 90% and increases as the input voltage increases. The fourth and sixth columns of Tables III and IV show that V_{dc} and V_{ac} correlate well as they both increase or decrease when each load increases or decreases, respectively. The same input voltage provides higher DC and AC output voltages under the low-loading condition (both 101Ω loads) compared to high-loading condition where both loads are 50.4Ω . This is expected under open-loop control, where both dual-output voltages have positive correlation with the load resistance. As expected, the input current as a negative relationship with the load resistance where the load current increases. But, adding the AC output port changes the expected DC output voltage on the DC port compared to well known equations. A method to theoretically predict the DC and AC output voltages is discussed in Section IV.

Comparing Tables V and III, or Tables VI and IV, the observations discussed above still hold even with “unbalanced” loads. The differences between values of each row in every single column are experimentally the same. Control of both the DC and AC output voltages is expected to be simultaneous since only one control signal is available and that is to switch the primary-side MOSFET.

TABLE III. Various input voltages for the balanced load $R_{dc}=R_{ac}=50.4\Omega$

Input Stage			DC Output		AC Output		Output Power (W)	η (%)
V_{in} (V)	I_{in} (A)	P_{in} (W)	V_{dc} (V)	I_{dc} (A)	V_{ac} (V)	I_{ac} (A)		
6.50	0.35	2.28	4.97	0.099	6.97	0.227	2.07	90.9
8.50	0.40	3.40	6.25	0.127	8.70	0.277	3.20	94.1
10.5	0.44	4.62	7.60	0.154	10.3	0.326	4.52	97.8
12.5	0.48	6.00	8.69	0.164	11.8	0.376	5.86	97.6

TABLE IV. Various input voltages for the balanced load $R_{dc}=R_{ac}=101\Omega$

Input Stage			DC Output		AC Output		Output Power (W)	η (%)
V_{in} (V)	I_{in} (A)	P_{in} (W)	V_{dc} (V)	I_{dc} (A)	V_{ac} (V)	I_{ac} (A)		
6.50	0.28	1.82	5.56	0.055	7.46	0.187	1.70	93.4
8.60	0.29	2.49	7.20	0.081	9.25	0.200	2.43	97.6
10.5	0.30	3.15	8.46	0.089	10.9	0.216	3.10	98.4
12.7	0.31	3.94	9.57	0.100	12.2	0.240	3.88	98.4

TABLE V. Various input voltages for the unbalanced load $R_{dc}=101\Omega$, $R_{ac}=50.4\Omega$

Input Stage			DC Output		AC Output		Output Power (W)	η (%)
V_{in} (V)	I_{in} (A)	P_{in} (W)	V_{dc} (V)	I_{dc} (A)	V_{ac} (V)	I_{ac} (A)		
6.60	0.34	2.25	5.50	0.059	7.29	0.252	2.16	96.0
8.60	0.37	3.18	6.88	0.068	8.77	0.300	3.10	97.5
10.7	0.40	4.28	8.08	0.081	10.3	0.349	4.25	99.3
12.8	0.44	5.63	9.21	0.090	12.0	0.399	5.61	99.6

TABLE VI. Various input voltages for the unbalanced load $R_{dc}=50.4\Omega$, $R_{ac}=101\Omega$

Input Stage			DC Output		AC Output		Output Power (W)	η (%)
V_{in} (V)	I_{in} (A)	P_{in} (W)	V_{dc} (V)	I_{dc} (A)	V_{ac} (V)	I_{ac} (A)		
6.50	0.30	1.95	5.01	0.110	7.28	0.164	1.75	89.7
8.50	0.33	2.80	6.41	0.132	9.10	0.199	2.66	95.0
10.6	0.35	3.71	7.81	0.159	10.6	0.215	3.52	94.9
12.6	0.37	4.66	9.02	0.200	12.1	0.232	4.61	98.9

Considering the ratio α between the AC output power and the total output power reflects the share of the AC port of the total output power. As shown in Table VII, α is almost constant for different input voltages under the same loading conditions. In the balanced load resistor cases, the AC output port takes up more output power than the DC output port with $\alpha \approx 75\%$. However in the unbalanced load resistor cases, this ratio moves in as expected above and below the 75% ratio to 85% with a high AC load (column six in Table VII) and 65% with a low AC load (column eight in Table VII).

Table VII. Ratio of AC output power to total output power (α)

$R_{dc}=R_{ac}=50.4\Omega$		$R_{dc}=R_{ac}=101\Omega$		$R_{dc}=101\Omega$, $R_{ac}=50.4\Omega$		$R_{dc}=50.4\Omega$, $R_{ac}=101\Omega$	
V_{in} (V)	α	V_{in} (V)	α	V_{in} (V)	α	V_{in} (V)	α
6.50	0.76	6.50	0.82	6.60	0.85	6.50	0.68
8.50	0.75	8.60	0.75	8.60	0.85	8.50	0.68
10.5	0.75	10.5	0.75	10.7	0.85	10.6	0.65
12.5	0.75	12.7	0.75	12.8	0.85	12.6	0.61

IV. MATHEMATICAL MODELLING

Modeling is essential to better understand the proposed topology including interaction between the input and output, and between the DC and AC output ports. In this section, only the ideal converter is considered compared to the non-ideal experiments presented in Section III. It is assumed that both the DC and AC output powers are completely dissipated in the resistive loads where other resistive elements, e.g. capacitor ESR, are ignored. The snubber circuit is also neglected since under ideal conditions all energy stored in the flyback transformer air gap is released to the dual-output ports in DCM.

Through the average input voltage and current waveforms in Fig. 4(a) and approximating the current non-zero portion as a triangle shown in Fig. 5,

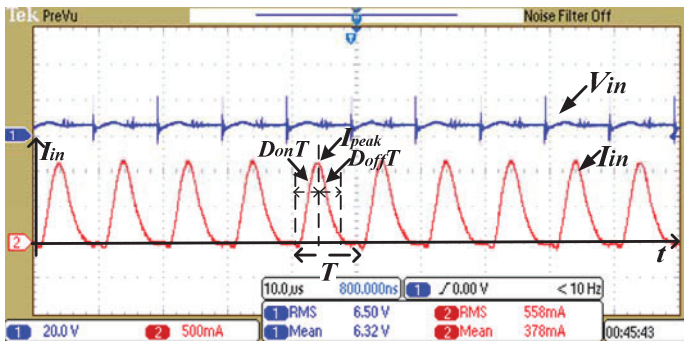


Fig.5. Modeling analysis of input current waveform

the average input energy into the flyback converter is,

$$E_{in} = \frac{1}{2} V_{in} (I_{peak} + I_o) (D_{on} + D_{off}) T, \quad (1)$$

where I_{peak} is the peak value of the input current—basically the value at the end of every switching ‘ON’ period, and I_o represents the returning input current value at the end of every switching cycle. Because the proposed flyback converter topology is operated in DCM, the input current returns to zero before the end of a switching cycle and thus I_o is always zero. T is one period time of switching cycle ($T=1/f$). D_{on} is the duty ratio of the MOSFET switching signal where the I_{in} increases to I_{peak} during $D_{on}T$, while D_{off} represents the portion of T during I_{in} decays from I_{peak} to zero. As mentioned earlier, D_{on} is roughly 35% rather than 50% and D_{off} is roughly 25%. Equation (1) can then be rewritten as,

$$E_{in} = \frac{1}{2} V_{in} \left(\frac{V_{in}}{L_m} D_{on} T \right) (D_{on} + D_{off}) T, \quad (2)$$

where the input energy only depends on the input voltage, on and off duty ratios, L_m , and the switching period as shown in equation (2) which is similar to that of conventional flyback converters. The sum of the DC and AC output ports’ energy is supposed to equal to this input energy value because of energy conservation and assuming an ideal converter. The total output energy becomes,

$$E_{total} = \frac{V_{ac}^2}{R_{ac}} T + \frac{V_{dc}^2}{R_{dc}} T. \quad (3)$$

Combining equations (2) and (3),

$$\frac{V_{in}^2}{2L_m} D_{on} (D_{on} + D_{off}) T^2 = \frac{V_{ac}^2}{R_{ac}} T + \frac{V_{dc}^2}{R_{dc}} T. \quad (4)$$

Canceling one T from both sides of equation (4),

$$\frac{V_{in}^2}{2L_m} D_{on} (D_{on} + D_{off}) T = \frac{V_{ac}^2}{R_{ac}} + \frac{V_{dc}^2}{R_{dc}}, \quad (5)$$

where right side of equation (5) is the combined DC and AC output power. Equations (4) and (5) are crucial to the proposed dual-output flyback converter, but the presence of two voltages in (5) requires further research into how they correlate for control and application purposes.

The LC low-pass filter alters the continuous square wave at the transformer secondary into a sinusoidal wave with zero-offset at the AC output port. More specifically, the LC low-pass filter blocks high frequency components and keeps the fundamental component in the Fourier series of the square wave. With the Fourier series of the square wave being,

$$S(t) = \frac{4}{\pi} \sum_{n=1,3,5}^{\infty} \frac{1}{n} \sin(n2\pi ft), \quad (6)$$

where $S(t)$ is the square wave with amplitude 1 and zero offset, f is its frequency which is the switching frequency in this topology. The fundamental component being V_{ac} with $n = 1$ is,

$$V_{ac}(t) = A \frac{4}{\pi} V_{in} \sin(2\pi ft), \quad (7)$$

where A is an unknown coefficient related to the load resistance and equation (7) shows the AC output voltage in the time domain. Therefore, the RMS value of the AC output voltage is,

$$V_{ac} = A \frac{4}{\sqrt{2\pi}} V_{in}, \quad (8)$$

Replacing V_{ac} in equation (5) by equation (8) and rearranging terms yields V_{dc} as,

$$V_{dc} = V_{in} \sqrt{\left(\frac{D_{on}(D_{on} + D_{off})T}{2L_m}\right)R_{dc} - \left(\frac{A^2 8}{R_{ac}\pi^2}\right)R_{dc}}. \quad (9)$$

Note that equation (9) is a positive relationship with the input voltage and the resistive load.

Comparison between theoretical and experimental values of V_{dc} is presented in Table VIII. Theoretical values are calculated using equations (5) and experimental values are presented in the Table III. Large error is observed at low V_{in} where the power efficiency is also lower than other cases and thus non-idealities are more dominant in the circuit. Therefore the DC output power is less than that from the proposed model leading to a lower experimental voltage. Because of undefined coefficient A in the equation (7), experimental values of V_{ac} are used in the theoretical calculations. More detailed comparisons are presented in the future work.

Table VIII. Theoretical values and experimental values of DC output voltage with balanced load $R_{dc}=R_{ac}=50.4\Omega$

Input Voltage V_{in} (V)	V_{dc}		Error
	Theoretical (V)	Experimental (V)	
6.50	5.76	4.97	13.8%
8.50	6.51	6.25	4.02%
10.5	7.28	7.60	-4.36%
12.5	9.14	8.69	4.91%

Further modeling research is necessary to better understand the dynamics of the proposed circuit, its component sizing, and its control strategies. Finding the AC output voltage coefficient (A) is also essential.

V. CONCLUSION AND FUTURE WORK

This paper presents a new topology of a dual-output flyback converter providing AC and DC voltages. Even though it could be applicable in various applications, the target application is rural renewable energy where high-frequency AC voltage can be used for fluorescent lighting in addition to the regular DC voltage for electronic loads. While other lighting options such as LEDs can replace the AC lighting in the long run, the latter is still more cost-effective especially in underdeveloped areas. Results show a proof-of-concept of the possible utilization of both AC and DC voltages from one flyback topology. They also show expected correlation to loading conditions. Understanding the operation and modeling is presented here, and the converter efficiency is shown to be high, especially if compared to topologies where dc-dc-ac conversion is cascaded. The proposed modeling approach shows low errors between the theoretical and measured DC output voltage. Future work will include focus on developing a non-ideal model, establishing a closed-loop control strategy for DC and/or AC output voltages, formalizing the capacitor and inductor sizing procedure, and applying the proposed topology in several applications at higher power ratings.

ACKNOWLEDGMENT

The authors would like to acknowledge the contribution of Julio Yela at the University of Connecticut for his early effort on this topic which helped identify some challenges.

REFERENCES

- [1] Siyang Zhao, Junming Zhang, and Yang Shi, "A low cost low power Flyback converter with a simple transformer," in *Proc. International Power Electronics and Motion Control Conference (IPEMC)*, 2012, pp.1336-1342, 2012.
- [2] Xiangjun Zhang, Hankui Liu, and Z. Xu, "Analysis and design of the flyback transformer," in *Proc. Annual Conference of the IEEE Industrial Electronics Society (IECON)*, 2003, pp.715-719.
- [3] N. Vazquez, H. Lopez, C. Hernandez, and H. Calleja, "Multiple-output DC-to-DC based on the flyback converter," in *Proc. IEEE International Power Electronics Congress*, 2008, pp. 105-108.
- [4] C.K. Huang, H.H. Nien, S.K. Changchien, C.H. Chan, and C.K. Chen, "An optimal designed RCD snubber for DC-DC converters," in *Proc. International Conference on Control, Automation, Robotics and Vision*, 2008, pp. 2202-2207.
- [5] W. McMurray, "Selection of Snubbers and Clamps to Optimize the Design of Transistor Switching Converters," in *IEEE Transactions on Industry Applications*, vol. IA-16, no.4, pp.513-523, July 1980.
- [6] G.N. Wooding and A.S. De Beer, "The effect of leakage inductance and snubbing on electromagnetic interference generated by a flyback converter," in *Proc. AFRICON*, 2011, pp.1-5.
- [7] L.M.K. Johny, and T.K.J. Sebastian, "A flyback DCM DC-AC converter for PV applications," in *Proc. Annual International Conference on Emerging Research Areas and 2013 International Conference on Microelectronics, Communications and Renewable Energy*, 2013, pp.1-6.
- [8] S. Howimanporm, and C. Bunlaksananusorn, "Performance comparison of continuous conduction mode (CCM) and discontinuous conduction mode (DCM) flyback converters," in *Proc. International Conference on Power Electronics and Drive Systems (PEDS)*, 2003, pp. 1434-1438.